


## Quantum nonstationary phenomena of spin systems in collision models

Yan Li, Xingli Li , and Jiasen Jin \*

*School of Physics, Dalian University of Technology, Dalian 116024, China*

 (Received 31 October 2022; accepted 31 March 2023; published 7 April 2023)

We investigate the nonstationary phenomenon in a tripartite spin-1/2 system in the collision model (CM) framework. After introducing the dissipation through the system-environment collision for both Markovian and non-Markovian cases, we find the emergence of long-time oscillation in the dynamics of the system and the synchronization among subsystems. We connect the CM description and the quantum master equation in the continuous-time limit and explain the existence of the stable oscillation by means of Liouvillian spectrum analysis. We investigate the thermodynamics of persistent oscillations in our CM in both Markovian and non-Markovian regimes. In addition, we find that the imperfection of collective dissipation can be compensated by the randomness of the interaction sequence in our CM.

DOI: [10.1103/PhysRevA.107.042205](https://doi.org/10.1103/PhysRevA.107.042205)

### I. INTRODUCTION

The quantum system that is subjected to coupling to an uncontrollable environment is referred to as an open quantum system. The inevitable interaction with the environment always leads to the dissipative effect of the open quantum system and the nonunitary feature of its time evolution [1–3]. In the presence or absence of memory effects, the dynamics of open quantum systems can be classified into the memoryless Markovian process and the non-Markovian master process which allows the backflow of information during the time evolution. In dissipative open quantum systems, in comparison with their closed counterparts, plenty of intriguing phenomena emerge, especially in the quantum many-body systems, such as the steady-state phase transition [4–7], information spreading [8–10], quantum many-body delocalization [11–14], etc. Generally, the state of an open quantum system asymptotically evolves to one or more time-independent steady states in the long-time limit. However, there are exceptional cases in which the system evolves to nonstationary states. The time-dependent long-time behavior of the system is intimately related to the quantum time crystals [15–17], quantum chaos [18,19], and quantum synchronization [20–24].

As the extension of classical synchronization in the quantum regime, quantum synchronization has attracted much attention in the last few years. The quantum synchronization between self-sustained oscillations can be established through either the external driving or the internal coupling [25–29]. The former is known as the forced synchronization or entrainment [30], while the latter is called spontaneous synchronization which stems from the quantum correlations in the systems. Meanwhile, the quantum correlations in the systems is not limited to direct interactions between subsystems, but also may emerge indirectly through the interactions of subsystems together with their surrounding environment.

These quantum correlations can eventually lead to nonstationary phenomena depicted by the quantum synchronization measure. In recent years, quantum synchronization in open quantum systems has been explored at length in a variety of quantum systems, such as optomechanical arrays [31–33], van der Pol (VdP) oscillators [28,34], atomic ensembles [35], and superconducting circuit systems [36–38].

In general, theoretic descriptions for the dynamics of open quantum systems as well as the nonstationary behavior in the long-time limit are carried out by calculating the expectation values of the local observables and correlations over time through the dynamical equations of the system such as the quantum master equation and quantum Langevin equation. In recent years, investigations of the open quantum system within the framework of the collision model (CM) have been reported [39–43]. The CM approach can provide intuitive pictures of the interactions between the system and its environment, as well as strategies of the information flows in the time evolution of the state of the system. Recently, it was shown that the CM can efficiently reproduce the dissipative collective phenomena of multipartite open quantum systems [44,45]. In the CM framework, the coupling of the system and environment is simulated by repeated collisions between the system and a set of environmental particles. Due to the flexibility and scalability in designing the collision details, the CM is a powerful tool for investigating non-Markovian dynamics [46–54], quantum information scrambling [55,56], quantum steering [57], quantum friction [58], multipartite entanglement generation [59], and quantum synchronization [30,60] in complicated open quantum systems. Recently, the experimental realization of an all-optical collision model has been demonstrated [61].

In this work, we utilize the CM to investigate the long-time behavior of a composite spin system consisting of three spin-1/2 subsystems subjected to a thermal environment. By varying the strength of the interactions within the environment blocks, we can obtain the Markovian dynamics and non-Markovian dynamics, respectively. We find that without

\*jsjin@dlut.edu.cn

additional external driving, the system is able to reach a stable nonstationary steady state only through its internal interactions and dissipative processes. At this point, synchronization phenomena are also constructed between subsystems, which is reminiscent of the results reported by Karpat *et al.* in Ref. [62]. Furthermore, after taking the continuous-time limit for the CM, we establish the connection between the CM and the Markovian master equation in Lindblad form. We interpret the appearance of the underlying long-time oscillations of the subsystems by analyzing the Liouvillian spectrum of the associated quantum master equation. In addition, we investigate the thermodynamical properties and correlations between the system and the environment when the dynamics of the subsystems are synchronized.

The paper is organized as follows. We first explain the idea of our specific model in the CM framework and its utility in simulating the dynamics of the composite systems consisting of three spins in Sec. II. In Sec. III, we then focus on the Markovian dynamics to show the temporal expectation values of the local observables. In particular for the case in which the subsystems enter into the long-time oscillations, we discuss the quantum synchronization among the subsystems. We explore the connection between the CM and Lindblad master equation in describing the underlying system in the continuous-time limit. We present our understanding of the appearance of oscillations in the dynamics from the Liouvillian spectrum, the thermodynamical properties, and the effects of imperfect collective dissipation on the dynamics. In Sec. IV, we discuss the time evolution of the systems in the non-Markovian case. Finally, we summarize in Sec. V.

## II. THE FRAMEWORK OF COLLISION MODEL

In the generic CM framework, the entire installation consists of two parts: the system  $\mathcal{S}$  and its environment  $E$ . Usually, the environment is represented by a set of identical particles denoted by  $\{E_1, E_2, \dots, E_j, \dots\}$ , which are initialized in the same state. The interaction between the system and the environment is simulated by the successive collisions between system particles and environmental particles in a stroboscopic manner. In our CM, both the system and environment consist of a set of spin-1/2 particles. In particular, the system of interest is tripartite with interacting subsystems  $S_1, S_2$ , and  $S_3$ . The inner interactions between the subsystems are given by (set  $\hbar = 1$  hereinafter)

$$H_S = \sum_{\alpha} \sum_{m=1}^3 J_{\alpha} \sigma_m^{\alpha} \sigma_{m+1}^{\alpha}, \quad (1)$$

where  $\sigma_m^{\alpha}$  ( $\alpha = x, y$ , and  $z$ ) are the Pauli matrices of the  $m$ th subsystem and  $J_{\alpha}$  is the coupling strength between the system spins. Notice that the periodic boundary condition is imposed in Eq. (1).

We consider the case in which the environmental spins are uncorrelated and are prepared in the identical thermal state  $\eta_{\text{th}}^j = e^{-\beta H_j} / \text{tr}(e^{-\beta H_j})$ ,  $\forall j$ . The free Hamiltonian of each environmental particle is  $H_j = \omega \sigma_j^z / 2$ , where  $\omega$  describes the self-energy and  $\beta = 1/k_B T$  is the inverse of temperature. Although the environment spins are initialized in the uncorrelated state, interactions between environment particles are

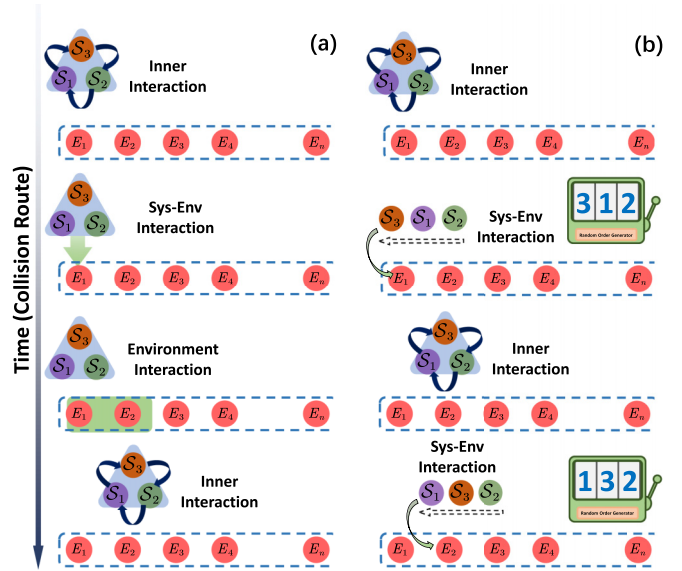


FIG. 1. Schematic of routes of collision models. (a) Collective dissipation: At the end of the interaction within the system, the tripartite system collides with the environment spin  $E_n$  simultaneously. (b) Random local dissipation. In this case, the subsystems collide with the environment blocks one by one and the interaction order is randomly determined each time.

allowed to take place. As will be seen in the next sections, it is the intra-environment interactions that generate the memory effect of the stroboscopic evolution of the system.

Now let us illustrate the setup of our CM, which is schematically shown in Fig. 1(a). The CM works through the following steps:

*Step 1.* The CM starts with the collisions among the subsystems  $S_1, S_2$ , and  $S_3$  according to Eq. (1). The time evolution of the state of the system is then described by the unitary operator  $U_S = \exp(-iH_S \tau_S)$  and  $\tau_S$  is the interaction time.

*Step 2.* Collisions take place between the system  $\mathcal{S}$  and environmental spin  $E_n$ . In this step, the  $\mathcal{S}$ - $E_n$  collision simulates the interaction between the system and environment, which is specified by the flip-flop Hamiltonian in our CM as follows:

$$H_I = g \sum_m \sigma_m^- \sigma_{E_n}^+ + \sigma_m^+ \sigma_{E_n}^-, \quad (2)$$

where  $g$  denotes the coupling strength of the system-environment interaction. The interaction shown in Eq. (2) describes the collective flip-flop process. This interaction is known as a good description for the collective spontaneous emission (Dicke superradiance) [63–65]. From an experimental point of view, this collective decay can be realized on the trapped-ion platform and mediated by an auxiliary ion [66,67]. The corresponding time-evolution operator is  $U_I = e^{-iH_I \tau_I}$ , where  $\tau_I$  denotes the interaction time.

*Step 3.* The collision takes place between the environment particles  $E_n$  and  $E_{n+1}$ , which may induce non-Markovian dynamics. The interaction Hamiltonian for the  $E_n$ - $E_{n+1}$  interaction reads

$$H_E = g_E \sum_{\alpha} \sigma_{E_n}^{\alpha} \sigma_{E_{n+1}}^{\alpha}, \quad (3)$$

where  $g_E$  is the coupling strength between environment spins. Thus, the unitary time-evolution operator can be expressed as  $U_E = e^{-iH_E \tau_E}$ , with  $\tau_E$  being the corresponding interaction time. Equation (3) can be reexpressed in the form of a partial SWAP operation,

$$U_E = \cos \theta \mathbb{I}_4 + i \sin \theta U_{\text{SWAP}}, \quad (4)$$

where  $\mathbb{I}_4$  is the  $4 \times 4$  identity operator and the SWAP operation is given by  $U_{\text{SWAP}} = |00\rangle\langle 00| + |01\rangle\langle 10| + |10\rangle\langle 01| + |11\rangle\langle 11|$ . The parameter  $\theta = 2g_E \tau_E$  controls the strength of the SWAP operation with  $\theta \in [0, \pi/2]$ . The non-Markovianity of the system dynamics can be switched on by tuning the parameter  $\theta$ .

After the  $E_n$ - $E_{n+1}$  collision, the spin  $E_{n+1}$  carries part of the information that flows into the environment in step 2. The system together with the  $(n+1)$ -th environment particle enters into the next loop and the spin  $E_n$  is discarded, as shown in Fig. 1(a). Therefore, the state of the system of interest after the  $n$ th loop ( $n \geq 2$ ) is transformed into

$$\rho_S^n \mapsto \rho_S^{n+1} = \text{tr}_{E_n, E_{n+1}} [U_E U_I U_S (\rho_{SE_n}^n \otimes \eta_{\text{th}}^{n+1}) U_S^\dagger U_I^\dagger U_E^\dagger], \quad (5)$$

where  $\rho_{SE_n}^n$  is the joint state of the system and the  $n$ th environment unit after collision. The system is initialized in the state  $\rho_S^{\text{ini}} = |\psi\rangle_S \langle \psi|$  with the separable state  $|\psi\rangle_S = |\psi\rangle_{S_1} \otimes |\psi\rangle_{S_2} \otimes |\psi\rangle_{S_3}$ . More precisely, since the Hamiltonian has the symmetry along the spin  $z$  axis, we choose the initial state of each subsystem as the  $120^\circ$  state on the equatorial plane of the Bloch sphere, i.e.,  $\psi_{S_m} = (|\uparrow\rangle + e^{im\frac{2}{3}\pi} |\downarrow\rangle) / \sqrt{2}$ , with  $m = 1, 2$ , and  $3$ . The chosen  $120^\circ$  state will facilitate the discussion of the evolution of the phase differences among the state of the subsystems. For simplicity, we set the interaction time for the each collision as  $\tau = \tau_S = \tau_I = \tau_E$  in the rest of the analysis.

### III. MARKOVIAN CASE

In this section, we focus on the case in which the intra-environment collision is absent in the CM, i.e.,  $U_E$  reduces to an identity matrix, implying that the dynamics of the system of interest is Markovian. We choose the temporal expectation value of local observable  $\langle \sigma_m^x \rangle = \text{tr}(\sigma_m^x \rho_S)$  to monitor the dynamics of the system. We first focus on the effect of the environmental temperature  $\beta$  on the time evolution of the state of the system. Note that  $\beta$  is proportional to  $1/T$ .

In Figs. 2(a) and 2(b), we show the time dependence of the local observables  $\langle \sigma_m^x \rangle$  for different  $\beta$ . One can see that the magnetizations of all the spins trivially approach to zero after a sufficiently large number of collisions for  $J_x = 3$  and  $\beta = 2$ . As the environmental temperature goes down, the asymptotic values of the magnetizations of all the spins become unstable, and eventually the time evolution of the magnetizations enter into the oscillating trajectories. The time-dependent oscillations of  $\langle \sigma_m^x(n) \rangle$  for  $\beta = 10$  can be observed in Fig. 2(b). Moreover, as shown in Fig. 2(c), the fast Fourier transform analysis on the numerics of  $\langle \sigma_m^x(n) \rangle$  reveals that the oscillations share the same dominant frequency. A zoom-in at the vicinity of the peak in the frequency domain shows that the dominant frequency is  $f^d \approx 0.32$ .

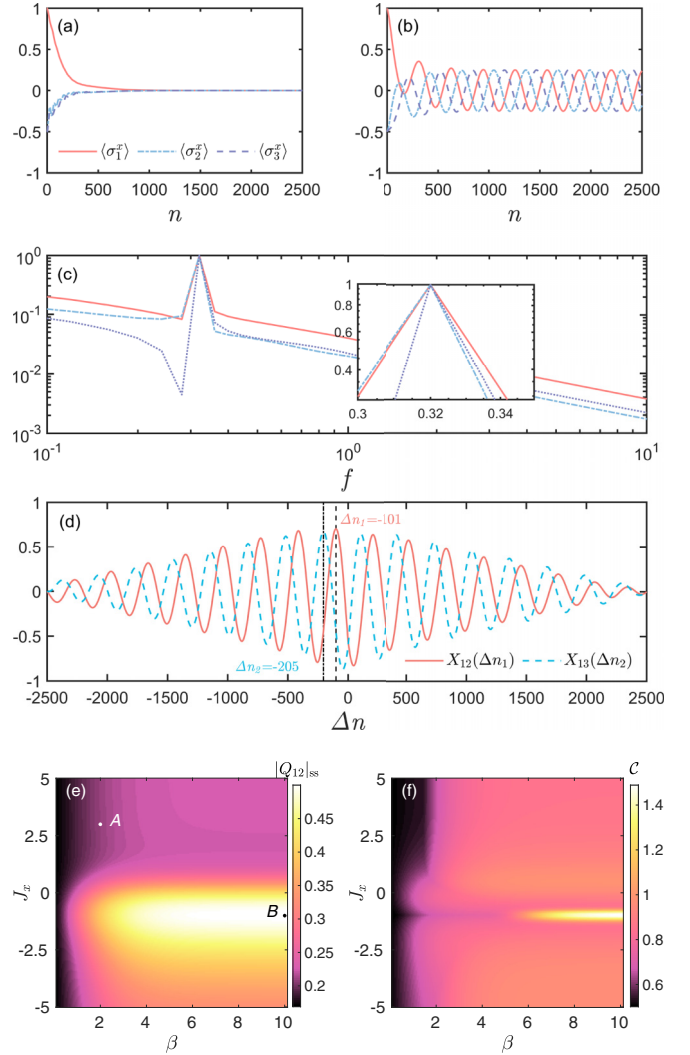


FIG. 2. The stroboscopic time evolution of the local observables  $\langle \sigma_m^x \rangle$  ( $m = 1, 2, 3$ ) with (a)  $J_x = 3, \beta = 2$  and (b)  $J_x = -1, \beta = 10$ . (c) The fast Fourier transform for the  $\langle \sigma_m^x \rangle$ s shown in (b); the zoom-in hints at those three local observables sharing an identical dominant frequency  $f^d \approx 0.32$ . (d) The cross correlations  $X_{1k}$ , ( $k = 2, 3$ ) of the  $\langle \sigma_m^x \rangle$ s shown in (b). (e) The absolute value of the synchronization measure  $Q_{12}(n)$  (computed up to  $n = 20000$  collisions) as a function of the environment temperature  $\beta = 1/k_B T$  and the coupling strength  $J_x$ . The black dots A and B mark the parameters ( $J_x = 3, \beta = 2$ ) and ( $J_x = -1, \beta = 10$ ), respectively. (f) The quantum coherence  $C$  in the system, as measured by the  $l_1$  norm of coherence; the parameters are chosen the same as in (e). Other parameters in all the panels are chosen as  $J_y = -1, J_z = 1, g = 10$ , and  $\tau = 0.01$ .

The phase-locking feature of the oscillations can be verified by checking the cross correlation between the time evolutions of  $\langle \sigma_m^x(n) \rangle$ . Generally, the cross correlation quantifies the degree of the association between these two time-dependent functions  $f(n)$  and  $g(n)$  and is defined as their convolutionlike function. Here, we analogously express the cross correlation for the discrete evolutions of  $\langle \sigma_m^x(n) \rangle$  as

$$X_{jk}(\Delta n) = \sum_{n=1}^N \langle \sigma_j^x(n) \rangle \langle \sigma_k^x(n - \Delta n) \rangle, \quad (6)$$

where  $\Delta n$  is the amount of translation and  $N$  is the total number of collisions. The cross-correlation function is actually an inner product of two vectors representing the projection of one onto another in the linear space. Therefore the cross correlation can faithfully capture the similarity of two vectors under different amounts of translation within a period. The maximum of  $X_{jk}(\Delta n)$  in Eq. (6) reveals the optimal translation that shifts the trajectory of  $\langle \sigma_j^x \rangle$  closest to  $\langle \sigma_k^x \rangle$  and thus in turn reflects the phase difference  $\Delta \phi_{S_j, S_k}$ . In Fig. 2(d), we show the cross correlation  $X_{jk}(\Delta n)$  produced by the data in Fig. 2(b); one can see that the maxima of the cross correlation  $X_{12}(\Delta n_1)$  and  $X_{13}(\Delta n_2)$  appear at  $\Delta n_1 = -101$  and  $\Delta n_2 = -205$ , respectively. Recall the previously calculated dominant frequency  $f^d \approx 0.32$ ; the phase differences can be obtained as  $\Delta \phi_{S_1, S_2} = 2\pi f^d / \Delta n_1 \tau \approx -2\pi/3$  and  $\Delta \phi_{S_1, S_3} = 2\pi f^d / \Delta n_2 \tau \approx -4\pi/3$ . The initial phase differences between the sublattices are conserved after the dissipative evolution. Note that we have rescaled the number of collisions,  $n$ , into time  $n\tau$  with time interval  $\tau = 0.01$ .

The phase-locking oscillation in the long-time dynamics of the system indicates the emergence of the spontaneous synchronization among the subsystems. In the following, we will employ the nonlocal synchronization measure proposed by Es'haqi-Sani *et al.* in Ref. [68] to quantify the synchronization features in our CM. The mentioned measure is a temporal complex-valued correlator and is defined as follows:

$$Q_{jk}(n) = \frac{\langle \sigma_j^+ \sigma_k^- \rangle_n}{\sqrt{\langle \sigma_j^+ \sigma_j^- \rangle_n \langle \sigma_k^+ \sigma_k^- \rangle_n}}, \quad (7)$$

where  $\langle O \rangle_n = \text{Tr}[O \rho_S^n]$  is the expectation value of the observable  $O$  after the  $n$ th collision. The modulus of  $Q_{jk}(n)$  characterizes the degree of nonlocal correlation; for instance, two subsystems are completely correlated when  $|Q_{jk}(t)| \rightarrow 1$ . Combining the dynamics of the local observable of the system and the behavior of this nonlocal correlation, we are able to investigate the synchronization properties. When the dynamics of the subsystems are oscillating and the nonlocal correlation function tends to a stable value, the subsystem can be considered to be synchronized. In Fig. 2(e), we show the modulus for the steady state  $|Q_{12}|_{ss}$  in the  $\beta - J_x$  plane. One can see that the lower environmental temperature ( $\beta \rightarrow \infty$ ) could facilitate the synchronization among the subsystems. Moreover, for  $\beta \geq 4$ , the long-time oscillation of the subsystems becomes almost fully synchronized at an optimal interaction strength  $J_x = J_y$ . Namely, the anisotropy of the system Hamiltonian tends to drive the dynamics of the subsystems far away from the synchronization.

On the other hand, the coherence property is also related to synchronization [69], which has already been considered as a synchronization measure [62,70]. In Fig. 2(f), we present the  $l_1$  norm of coherence of the state of the system in the  $\beta - J_x$  plane. The  $l_1$  norm of coherence is defined as follows:

$$C = \sum_{p \neq q} |\langle p | \rho_S | q \rangle|, \quad (8)$$

where  $\{|p\rangle\}$  are the computational basis of  $\rho_S$  [71]. Indeed, we find that there are many similar behaviors in Figs. 2(e) and 2(f). For a lower environmental temperature or an anisotropic Hamiltonian, the coherence of the system is poorly present

in the system, which implies that the synchronization is more likely to be established when the state of system  $\rho_S$  contains more coherence.

### A. Continuous-time limit

In the preceding, we have found that the emergence of the synchronization depends on both the properties of the system Hamiltonian and the environment temperature. In order to figure out the underlying physics, we are going to analyze the dynamics of the system by taking the continuous-time limit for the Markovian CM. We start with a discussion of a single loop, say, the  $n$ th loop, in a more general CM with the system-environment interaction Hamiltonian in the form of  $V = g \sum_k \mathcal{A}_k \otimes E_k$ , where  $\mathcal{A}_k$  and  $E_k$  are the operators of the system and environment spins. Notice that since we are only concerned with the final state of the system after the  $n$ th loop in the Markovian CM, the collision between  $E_n$  and  $E_{n+1}$  is not considered for the moment. The map for the system state is thus given by

$$\rho_S^n \mapsto \rho_S^{n+1} = \text{tr}_{E_{n+1}} [U_I U_S (\rho_S^n \otimes \eta_{th}^{n+1}) U_S^\dagger U_I^\dagger] = \Lambda[\rho_S^n], \quad (9)$$

where  $\Lambda[\cdot]$  is a completely positive trace-preserving (CPTP) map acting on the system density matrix  $\rho_S$  and  $U_I = e^{-iV\tau}$  is a unitary operator describing the collision between the system and environment. In the continuous-time limit ( $\tau \rightarrow 0$ ), we can expand the unitary operators as follows:

$$U_I = \mathbb{I} - i\tau V - \tau^2 V^2 / 2 + o(\tau^n) \quad (10)$$

and

$$U_S = \mathbb{I} - i\tau H_S + o(\tau^n). \quad (11)$$

Therefore, the variation of  $\rho_S$  between two consecutive loops can be obtained as follows:

$$\delta \rho_S = \rho_S^{n+1} - \rho_S^n = (\Lambda - \mathbb{I})[\rho_S^n]. \quad (12)$$

By substituting Eqs. (A2) and (A3) into Eq. (12), we have

$$\begin{aligned} \delta \rho_S \approx & -i\tau [H_{SS}, \rho_S^n] + \frac{\tau^2}{2} \text{tr}_E (2V \rho_S^n \otimes \eta_{th}^{n+1} V \\ & - \{V^2, \rho_S^n \otimes \eta_{th}^{n+1}\}) - i\tau \text{tr}_E ([V, \rho_S^n \otimes \eta_{th}^{n+1}]) \\ & - \tau^2 \text{tr}_E (\{\rho_S^n \otimes \eta_{th}^{n+1}, H_S V\}) - \tau^2 \text{tr}_E (V \rho_S^n \otimes \eta_{th}^{n+1} H_S \\ & - H_S \rho_S^n \otimes \eta_{th}^{n+1} V). \end{aligned} \quad (13)$$

Under the assumptions  $\text{tr}_E [\eta_{th}^{n+1} V] = 0$  and  $\text{tr}_E [\eta_{th}^{n+1} V^2] \neq 0$ , which is trivially satisfied in the cases in which the initial environment states have zero first-order moment, we divide both sides of Eq. (13) by the collision time  $\tau$  and may obtain the following quantum master equation in Lindblad form:

$$\begin{aligned} \frac{d}{dt} \rho_S(t) = & -i[H_S, \rho_S] + \frac{g^2 \tau}{2} \sum_{k,l} \Gamma_{k,l} (2\mathcal{A}_k \rho_S \mathcal{A}_l \\ & - \{\mathcal{A}_l \mathcal{A}_k, \rho_S\}), \end{aligned} \quad (14)$$

where  $\Gamma_{k,l} = \langle E_l E_k \rangle_{\eta_{th}^{n+1}}$  is the environment correlation function and the dimensionless parameter  $g^2 \tau$  is the effective decay rate. In our CM, the jump operators in Eq. (14) are



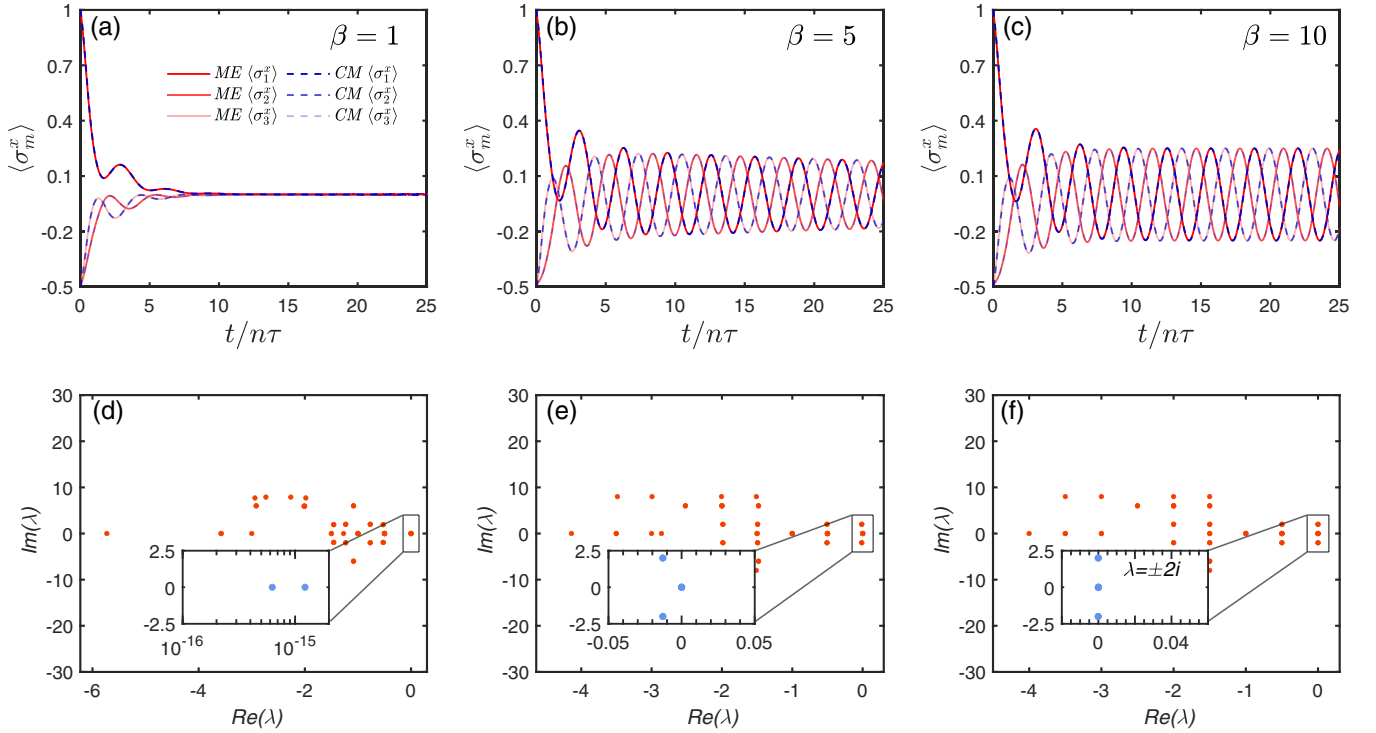


FIG. 3. Top panels: The time evolution of the expectation values  $\langle \sigma_m^x \rangle$  ( $m = 1, 2, 3$ ) of the system  $\mathcal{S}$  (different subsystems are distinguished by the transparency of the line) in the description of the master equation (solid lines) and collision model (dashed lines). Bottom panels: The Liouvillian spectra in the complex planes. The environmental temperatures are (a),(d)  $\beta = 1$ , (b),(e) 5, and (c),(f) 10. All of the zoom-ins show the details of the eigenvalues around the zero real part. Other parameters are chosen as  $J_x = J_y = -1$ ,  $J_z = 1$ ,  $\gamma = 1$ ,  $g = 10$ , and  $\tau = 0.01$  for all the panels.

determine to be the collective lowering and raising operators  $A^\pm = \sum_m \sigma_m^\pm$ , and we end up with the master equation in the Lindblad form,

$$\begin{aligned} \frac{d}{dt} \rho_S(t) = & -i[H_S, \rho_S(t)] + \frac{\gamma(1-\xi)}{4} [2A^- \rho_S(t) A^+ \\ & - \{A^+ A^-, \rho_S(t)\}] + \frac{\gamma(1+\xi)}{4} [2A^+ \rho_S(t) A^- \\ & - \{A^- A^+, \rho_S(t)\}], \end{aligned} \quad (15)$$

where  $\xi = \tanh(-\beta\omega)$  is the environment correlation function and  $\gamma = g^2\tau$  describes the decay rate. Moreover, it is important to emphasize that when the temperature of the environment state is low ( $\xi \rightarrow -1$ ), we can eventually obtain the master equation in a vacuum environment,

$$\frac{d}{dt} \rho_S(t) = -i[H_S, \rho_S(t)] + \frac{\gamma}{2} [2A^- \rho_S(t) A^+ - \{A^+ A^-, \rho_S(t)\}]. \quad (16)$$

To corroborate the equivalence between the CM and quantum master equation descriptions for different temperatures, we show the stroboscopic and continuous-time evolution of  $\langle \sigma_m^x \rangle$  for the subsystems in Figs. 3(a)–3(c). Note that the timeline for the CM has been rescaled to  $t = n\tau$ . One can see that the results calculated through both descriptions agree well with each other in the continuous-time limit  $\tau \rightarrow 0$ , regardless of the temperature of the environment. Moreover, we observe again that the synchronization of the subsystems is established when the temperature of the environment is low. In the case of

the vacuum environment, the synchronized oscillations of the local observable of each subsystem always persist.

## B. Liouvillian spectrum

So far, we have verified the equivalence between the CM and master equation descriptions for the Markovian dynamics of open systems. In this section, we will concentrate on the case of vacuum environment since the oscillations in the dynamics survive in the long-time limit. Actually, the Lindblad master equation (16) always hints at a linear CPTP map, which can be described as  $\frac{d}{dt} \rho_S(t) = \mathcal{L}[\rho_S(t)]$ , where  $\mathcal{L}[\cdot]$  is the Liouvillian superoperator acting on the density matrix of the system. The Liouvillian  $\mathcal{L}$  is the generator of the dynamics semigroup  $e^{\mathcal{L}t}$  ( $t \geq 0$ ). This reminds us to figure out the origin of the synchronization in our model via the symmetry of the Liouvillian.

In Fock-Liouville space, the Liouvillian can be recast in a non-Hermitian matrix  $\bar{\mathcal{L}}$  as follows:

$$\begin{aligned} \bar{\mathcal{L}} = & -i[(H \otimes \mathbb{I}) - (\mathbb{I} \otimes H^T)] \\ & + \frac{\gamma}{2} (2L \otimes L^* - L^\dagger L \otimes \mathbb{I} - \mathbb{I} \otimes L^T L^*), \end{aligned} \quad (17)$$

where  $\mathbb{I}$  denotes the identity operator and  $L$  is the corresponding jump operator in the master equation (the superscript T denotes the transpose of the matrix). The eigenvalue decomposition on the Liouvillian matrix reads [72,73]

$$\bar{\mathcal{L}}|\rho_j\rangle\rangle = \lambda_j|\rho_j\rangle\rangle, \quad (18)$$

where  $|\rho_j\rangle\rangle$  are the eigenvectors and  $\lambda_j$  are the associated complex eigenvalues. The real parts of the eigenvalues  $\lambda_j$  are always negative semidefinite and can be sorted in descending order as  $0 \geq \text{Re}[\lambda_0] > \text{Re}[\lambda_1] > \text{Re}[\lambda_2] > \dots > \text{Re}[\lambda_n]$ . An arbitrary initial state can always be represented in a superposition of  $\rho_j$  as  $\rho_S(0) = \sum_j c_j \rho_j$ , where  $c_j$  is the probability amplitude. Therefore, at any time  $t > 0$ , the system evolves to the following state:

$$\rho_S(t) \propto \frac{\rho_0}{\text{tr}(\rho_0)} + \sum_{j \neq 0} c_j e^{\lambda_j t} \rho_j. \quad (19)$$

It is obvious that the eigenstate  $\rho_0$ , which is associated with the zero eigenvalues, i.e.,  $\text{Re}[\lambda_0] = \text{Im}[\lambda_0] = 0$ , will remain unchanged and is the asymptotic steady state. On the other hand, the components in the summation will vanish in the long-time limit ( $t \rightarrow \infty$ ) because of the negative real part of  $\lambda_j$ . However, it is remarkable that the pure imaginary eigenvalues,  $\text{Re}[\lambda_j] = 0$  and  $\text{Im}[\lambda_j] \neq 0$ , may protect the corresponding eigenstates from decaying and lead to a persistent oscillation with time. Therefore, the emergence of the oscillations of the local observables stems from the appearance of the pure imaginary eigenvalues of the underlying Liouvillian superoperator.

In Figs. 3(d)–3(f), we show the Liouvillian spectra in the complex plane. One can see that the eigenvalues are always symmetrically distributed about the real axis ( $\text{Im}[\lambda] = 0$ ). We are interested in the eigenvalues with large real parts that are close to the imaginary axis. As shown in Fig. 3(d), zero eigenvalues exist for high temperature  $\beta = 1$ , indicating the existence of the asymptotic steady states. Note, also, that zero eigenvalues have degenerated. As the temperature lowers, a pair of conjugate eigenvalues gets closer to the imaginary axis, as shown Fig. 3(e). Although the dynamics of the system is yet a damped oscillation, it is a precursor of the birth of persistent oscillations in the dynamics. For  $\beta = 10$ , we observe a pair of conjugated pure imaginary eigenvalues  $\lambda = \pm 2i$  which is responsible for the emergence of the persistent oscillation in the dynamics. Moreover, according to Eq. (19), we are able to deduce the frequency of the oscillation as  $f = |\pm 2i|/2\pi \approx 0.32$ , which is consistent with the fast Fourier transform (FFT) analysis in Fig. 2(c).

### C. The structure of the steady-state density matrix

As mentioned in Eq. (19), the long-time density matrix of the system is constructed of the eigenstates of the Liouvillian associated to the eigenvalues with vanishing real parts. In particular, the long-time oscillating behavior of the system requires the basis matrix  $M_j$  of the density matrix satisfying

$$[M_j, H_S] = m_j M_j, \quad [A^-, M_j] = [A^+, M_j] = 0, \quad (20)$$

where  $m_j$  is real [74,75].

In our CM, the equivalent master equation (16) always has a fixed solution with all spins pointing down along the  $z$  direction, i.e.,  $|\psi_\downarrow\rangle = |\downarrow\downarrow\downarrow\rangle$ , corresponding to the eigenenergy  $\varepsilon_\downarrow$ . Meanwhile, the Hamiltonian of the system has at least one pair of degenerate eigenstates  $|\psi_m\rangle$  and  $|\psi_n\rangle$  with  $\varepsilon_m = \varepsilon_n$ . These two degenerate eigenstates together with the state  $|\psi_\downarrow\rangle$  can construct nine eigenoperators:  $M_1 = |\psi_m\rangle\langle\psi_m|$ ,  $M_2 = |\psi_n\rangle\langle\psi_n|$ ,  $M_3 = |\psi_\downarrow\rangle\langle\psi_\downarrow|$ ,  $M_4 = |\psi_m\rangle\langle\psi_n|$ ,  $M_5 = |\psi_n\rangle\langle\psi_m|$ ,

$M_6 = |\psi_\downarrow\rangle\langle\psi_m|$ ,  $M_7 = |\psi_\downarrow\rangle\langle\psi_n|$ ,  $M_8 = |\psi_n\rangle\langle\psi_\downarrow|$ , and  $M_9 = |\psi_m\rangle\langle\psi_\downarrow|$ , which fulfill the requirements in Eq. (20). As a consequence, we can obtain the equation of the dynamics of those eigenoperators as

$$\frac{d}{dt} M_j = -im_j M_j = -i(\varepsilon_l - \varepsilon_k) |\psi_l\rangle\langle\psi_k|, \quad l, k = \downarrow, m, n. \quad (21)$$

The matrices  $M_1, \dots, M_5$  are the dark states in the dynamical process; matrices  $M_6, \dots, M_9$  denote the mixed coherence oscillation. Choosing the same parameter as in Fig. 3, we can obtain a pair of degenerate eigenstates with  $p_n = p_m = 3$  and  $p_\downarrow = 1$ . In the long-time limit, the system eventually evolves in the eigenstate subspace consisting of  $|\psi_n\rangle$ ,  $|\psi_m\rangle$ ,  $|\psi_\downarrow\rangle$ , and oscillates in the following ways:  $|\psi_n\rangle \leftrightarrow |\psi_\downarrow\rangle$  and  $|\psi_m\rangle \leftrightarrow |\psi_\downarrow\rangle$  with the frequencies  $f_{n\leftrightarrow\downarrow} = f_{m\leftrightarrow\downarrow} = |p_{n,m} - p_\downarrow|/2\pi \approx 0.32$ , consistent with the previous results.

Actually, the conditions in Eq. (20) suggest that the emergence of persistent oscillations is supported by the so-called strong dynamical symmetry of the system. To be specific, in Eq. (20), the former commutator defines a dynamical symmetry of the autonomous evolution of the system, while the latter commutator ensures that such dynamical symmetry survives in the presence of dissipation [75,76]. Recently, the dynamical symmetry has been shown to be powerful in analyzing the properties of the limit cycles in the dynamics of the open quantum system, for example, the antisynchronization in a three spin-1/2 system (with one of the spins acting as a bath) [77], and the robustness of the persistent oscillations in a periodically arranged four-site spin chain in a collision model with random time for the system's autonomous evolution [76].

In particular, as shown in Ref. [76], the CPTP map in Eq. (9) can be described by the time-evolution and Kraus operators, without taking the continuous-time limit for the derivation of the Lindblad master equation; the oscillation frequency is unrelated to any timescale of the system-environment interaction and is just of a matter of the spectrum of the CPTP map. As will be seen in the ultrastrong non-Markovian case, the failure of the composition of CPTP maps in describing the time evolution breaks the persistence oscillation in our CM in the ultrastrong non-Markovian case.

### D. Entropy and correlations

In this section, we discuss the dynamics of the system from the thermodynamic viewpoint. In the general description of the dynamics of an open quantum system, the nonunitary time evolution of the state of the system of interest is given by the following dynamical map, given the initial state of the system as  $\rho^{\text{ini}}$ :

$$\rho_S^{\text{ini}} \mapsto \rho_S(t) = \text{tr}_E[U(t)(\rho_S^{\text{ini}} \otimes \eta_{\text{th}})U^\dagger(t)], \quad (22)$$

where  $U(t)$  is the unitary time evolution of the system and environment and  $\text{tr}_E$  is the partial trace taken over the degree of freedom of the environment. In Eq. (22), it is assumed that the system is uncorrelated with the environment at the initial time and the environment is in the thermal state characterized by a temperature. Note that a constant temperature makes sense only in the thermodynamic limit, i.e., when the number of degrees of freedom approaches infinity. In the CM,

such thermal environment is represented by a set of qubits that collide with systems at each step. Thus, the state of the system is stroboscopically transformed as  $\rho_S^{n-1} \rightarrow \rho_S^n$  at each step, which can be implemented by only involving the  $n$ th environment qubit. The specific form of the time evolution in the CM simplifies the computation of the dynamics of open systems and makes the formulation of thermodynamics in the CM tractable.

One can formulate the thermodynamics in each step of the CM. For example, the entropy production  $\Sigma^n$  in the  $n$ th step is given by  $\Sigma^n = \Delta S^n + \Phi^n$ , where  $\Delta S^n = S(\rho_S^n) - S(\rho_S^{n-1})$  ( $\rho_S^0$  is the initial state) is the entropy increment of the system after time evolution with  $S(\rho) = -\text{tr}(\rho \ln \rho)$  the von Neumann entropy, and  $\Phi^n = \beta \Delta Q_E^n = \beta \text{tr}[H(\rho_E^n - \eta_{\text{th}}^n)]$  is entropy flux after the  $n$ th system-environment interaction. But one should pay special attention to the fact that  $\Sigma^n$ ,  $\Delta S^n$ , and  $\Phi^n$  are defined as the corresponding thermodynamic quantities in a single step of the CM and only the environmental qubits that couple to the system in this step can be used to calculate these thermodynamic quantities. Recall that the thermal environment in the CM consists of all the environmental qubits, in which a thermodynamic quantity (entropy production, work, heat, etc.) up to a time  $t = n\tau$ , with  $\tau$  being the time interval between two successive collisions, should be the cumulative sum of the same quantity per step up to the  $n$ th step [78–80]. Therefore, the entropy production after  $n$  steps of the CM reads

$$\Sigma(n) = \Delta S(n) + \Phi(n), \quad (23)$$

with the cumulated thermodynamic quantity defined by  $A(n) = \sum_{j=1}^n A^j$ . We noticed that when the persistent oscillation is absent in the long-time limit, the entropy production for the  $n$ th step can be interpreted as the entropy production rate by simply reexpressing  $\Sigma^n$  as  $\Sigma^n = \Sigma(n) - \Sigma(n-1)$ . It is shown that the entropy production is equal to a relative entropy and thus, by construction, is positive [78–80]. Nevertheless, the entropy production rate need not be positive and the Landauer's principle by means of the entropy production rate has been discussed in Refs. [81,82]. Since we are interested in the case in which the persistent oscillation is present in the long-time limit, and the physical meaning of  $\Sigma^n$  is not well understood, we will focus on the cumulative quantities in the following.

In Fig. 4(a), we show the time evolutions of the relevant thermodynamic quantities in our CM for the case in which the long-time oscillation survives. One can see that all quantities are always positive after each collision step, especially the entropy production. The always-positive entropy production shows that the system always obeys Landauer's principle, and the second law of thermodynamics is not violated.

In addition, the entropy production keeps increasing monotonically and remains constant after the system gradually establishes stable oscillations [combined with the results of  $\langle \sigma_1^x \rangle$  in Fig. 4(b)]. This can be understood as the following. On the one hand, it is the coupling to the environment that leads the entropy production to rise and go to a constant (the value is proportional to the coupling strength). On the other hand, due to the dynamical symmetries, as presented in Eq. (20), there is a subspace of the system that is effectively decoupled from

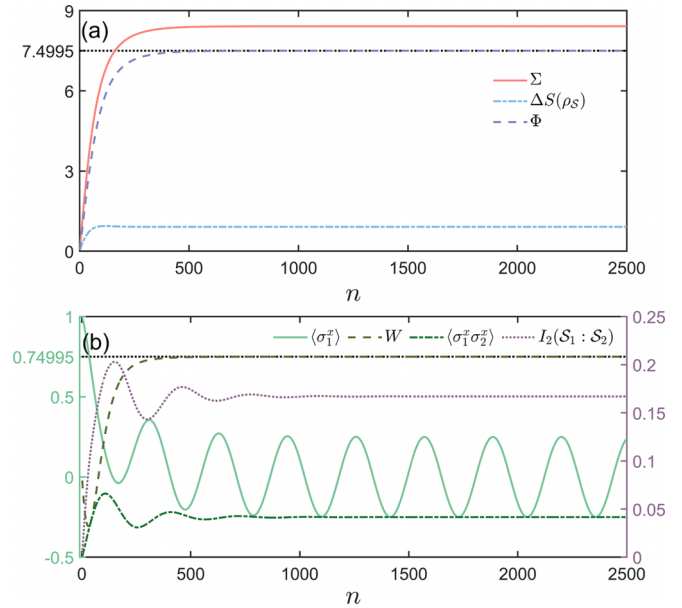


FIG. 4. (a) The  $n$  dependence of the entropy production  $\Sigma$ , entropy increment of the system  $\Delta S(\rho_S)$ , and entropy flux  $\Phi$ ; all results are obtained through Eq. (23). (b) The  $n$  dependence of expectation  $\langle \sigma_1^x \rangle$  (left y axis), the work  $W$  (left y axis), the two-point spin-spin correlation function  $\langle \sigma_1^x \sigma_2^x \rangle$  (left y axis), and the bipartite mutual information of sublattices  $I_2(S_1 : S_2)$  (right y axis). The parameters for the two panels are chosen as  $J_x = J_y = -1$ ,  $J_z = 1$ ,  $g = 10$ ,  $\beta = 10$ , and  $\tau = 0.01$ .

the environment throughout the time evolution. The remaining subspace couples to the environment and approaches to an asymptotic steady state in the long-time limit. The contributions from both subspaces lead the observables to oscillate persistently.

In our CM, the total energy of the system is not conserved due to  $[H_S, H_I] \neq 0$ . It means that the work  $W$  may be performed during the whole evolution process [78,83]. According to the first law of thermodynamics, the work up to the  $n$ th step is defined by the mismatch of the internal energy of the system  $\Delta U$  and the heat  $\Delta Q_E$  dissipated to the environment as  $W(n) = \Delta U(n) + \Delta Q_E(n)$ . Again, the internal energy up to the  $n$ th step,  $\Delta U(n) = \sum_{j=1}^n \Delta U^j$ , is the cumulation of the change in internal energy at each step,  $\Delta U^j = \text{tr}[H_S(\rho_S^j - \rho_S^{j-1})]$ .

Here we show the results of the work in Fig. 4(b). The plus or minus signs of  $W$  mean the energy is either poured into or extracted from the system, respectively. In Fig. 4(b), we compare the time-evolution value of  $W$  and the expectation value  $\langle \sigma_1^x \rangle$ . One can see that at the beginning of the evolution, the value of the work is taken as negative. This behavior corresponds to the rapid dissipation of the system energy into the environment, which is in accordance with the rapid decay of  $\langle \sigma_1^x \rangle$ . Then, after a short evolutionary process up to the time  $t = n\tau \approx 6$ , the work rapidly approaches a constant. Comparing with the numerics of the steady-state value of the entropy flux in Fig. 4(a), we find that the work is equal to the heat  $W = \sum_j \Delta Q_E^j = \Phi/\beta$ , namely, the energy poured into the system happens to be completely dissipated into the environment. We note that the initial state of system is chosen

as the  $120^\circ$  state mentioned in Sec. II. In this case, after the system undergoes long-term evolution, the internal energy of the system is completely consistent with that of the system at the initial time.

Although a subspace of the system has decoupled from its environment, the system does not enter into a stable oscillation immediately ( $\langle \sigma_1^x \rangle$  has not yet reached a stable oscillation when the work reaches constant). This can be attributed to the fact that the establishment of the long-time oscillation is not only induced by the dissipation, but is also a result of the self-adjusting of the correlations among the subsystems. The evidence can be found in the time evolutions of the correlator  $\langle \sigma_1^x \sigma_2^x \rangle$  and the bipartite mutual information  $I_2(\mathcal{S}_1 : \mathcal{S}_2) = S(\rho_{\mathcal{S}_1}) + S(\rho_{\mathcal{S}_2}) - S(\rho_{\mathcal{S}_1, \mathcal{S}_2})$ . As shown in Fig. 4(b), both  $\langle \sigma_1^x \sigma_2^x \rangle$  and  $I_2(\mathcal{S}_1 : \mathcal{S}_2)$  approach the steady-state values simultaneously with the establishment of the stable oscillations at  $n \approx 1200$ .

### E. Imperfect interaction

So far, we have considered that the system-environment interaction is in the collective fashion, namely, the three system spins interact with the environment particle at the same time. However, from the experimental point of view, it is difficult to realize the simultaneous interactions between the system and the environment spins. A more realistic scenario is that the system spins interact with the environment spin sequentially in a fixed order, e.g.,  $\mathcal{S}_1-E_n \rightarrow \mathcal{S}_2-E_n \rightarrow \mathcal{S}_3-E_n$ . The system-environment collision in the sequential way is thus ruled by the unitary operator  $U_{I,123}^{\text{seq}} = U_{\mathcal{S}_3 E_n} U_{\mathcal{S}_2 E_n} U_{\mathcal{S}_1 E_n}$ , with  $U_{\mathcal{S}_m E_n} = \exp[-ig\tau(\sigma_{\mathcal{S}_m}^+ \sigma_{E_n}^- + \text{H.c.})]$  ( $m = 1, 2, 3$ ). Following the expansion method mentioned in the Sec. III A, we can obtain the master equation for the sequential collision case. We show the details of derivation in the Appendix.

In Fig. 5(a), we show the stroboscopic evolution of  $\langle \sigma_1^x \rangle$  in the CM where system-environment interactions act sequentially in various orders (labeled by the subscripts of the time-evolution operators  $U^{\text{seq}}$ ). In contrast to the case of collective interactions, the oscillations of  $\langle \sigma_1^x \rangle$  are observed in the initial stage of the time evolution for all  $U^{\text{seq}}$ s, while as time passes, the amplitudes of the oscillations are suppressed and the magnetization  $\langle \sigma_1^x \rangle$  asymptotically decays to zero. We show the Liouvillian spectrum for the case in which the time-evolution operator is  $U_{I,123}^{\text{seq}}$  in the inset of Fig. 5(a). One finds the largest real part of the eigenvalue of the Liouvillian to be  $\text{Re}[\lambda_1] = 0.0115$  and the magnetization  $\langle \sigma_1^x \rangle$  asymptotically decays to zero within the timescale  $\sim 1/\text{Re}[\lambda_1]$ .

However, the subsystem spins interact with the environment spin sequentially in a fixed order during the entire evolution, which is still demanding for experimental realization. We now investigate the effects of the imperfections of the interaction order on the dynamics of the system. We simulate the imperfections by randomly permuting the system spins in the queue at each step. As shown in Fig. 5(b), it is interesting that the random orders of interaction between the system and environment spins significantly prolong the oscillations and even recover the behavior of  $\langle \sigma_1^x \rangle$  appearing in the case in which the system spins collectively interact with the environment spin.

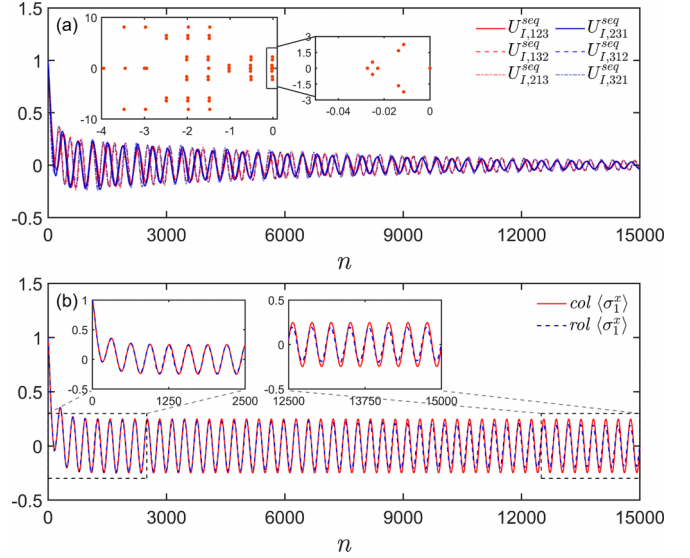


FIG. 5. (a) The stroboscopic evolution of  $\langle \sigma_1^x \rangle$  in collision models with different sequences in the system-environment collision. The zoom-in shows the Liouvillian spectrum of the  $U_{I,123}^{\text{seq}}$  case. (b) The stroboscopic evolution expectation values of  $\langle \sigma_1^x \rangle$  in the collision models with collective system-environment collision (red line) and individual subsystem-environment collisions in random order (blue line). The parameters are chosen as  $J_x = J_y = -1$ ,  $J_z = 1$ ,  $g = 10$ ,  $\tau = 0.01$ , and  $\beta = 10$ .

To address this point, we recall the sequential collision master equation shown in the Appendix. Comparing with Eq. (16), one finds that some additional terms appear in Eq. (A6) which are determined by the collision sequence. These extra terms will be mixed destructively due to the rapid permutation of the subsystems in the system-environment interaction during the whole time evolution. For instance, the term  $\sigma_1^+ \sigma_3^- \rho_S(t)$  appearing in the  $\mathcal{S}_1-E_n \rightarrow \mathcal{S}_2-E_n \rightarrow \mathcal{S}_3-E_n$  sequence cancels the term  $-\sigma_1^+ \sigma_3^- \rho_S(t)$  appearing in the  $\mathcal{S}_3-E_n \rightarrow \mathcal{S}_2-E_n \rightarrow \mathcal{S}_1-E_n$  sequence. Therefore, in the short-term evolution, the time evolution of  $\langle \sigma_1^x \rangle$  in the random collision strategy agrees well with that in the collective collision strategy. However, after sufficiently long time, the difference between the two cases is accumulated so that the amplitude of the oscillation differs.

### IV. NON-MARKOVIAN CASE

We turn to the non-Markovian case in this section by switching on the interaction between neighboring environmental spins. As we mentioned in Sec. II, in the CM framework, the non-Markovian dynamic can be implemented by introducing the inner collision between the environment spins  $U_E$ . The idea is the following: At the collision step  $n$ , the system  $\mathcal{S}$  collides with the environment spin  $E_n$ , and the information from the system partially flows into the environment. Then the environment inner collision takes place, and the environment spin  $E_n$  collides with the fresh environment spin  $E_{n+1}$ . In this way, the spin  $E_{n+1}$  also partially carries the system information. In the next collision step  $n + 1$ , when a collision happens between the system  $\mathcal{S}$  and the environment



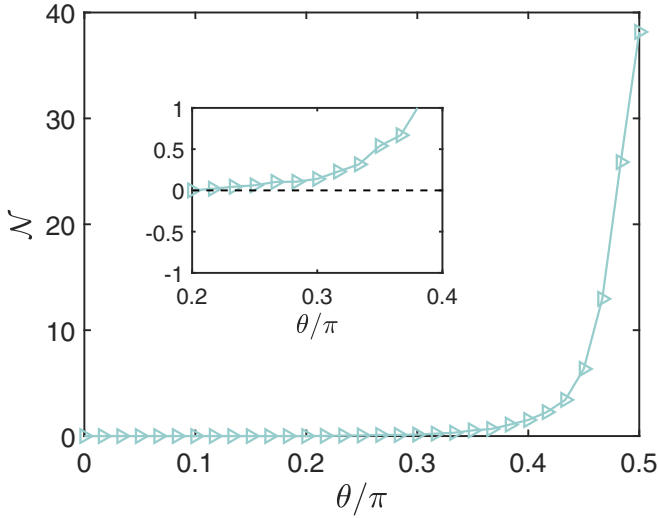


FIG. 6. The degree of non-Markovianity as a function of  $\theta/\pi$ . The number of collisions is  $n = 500$ . Other parameters are chosen as  $J_x = J_y = -1, J_z = 1, \beta = 10, g = 5$ , and  $\tau = 0.08$ .

$E_{n+1}$ , the information that flowed into the environment has the possibility to flow back to the system.

Although the  $E_n-E_{n+1}$  collision enables the information backflow, a measure still needs to quantify the degree of the non-Markovianity of the dynamics of the system. To this aim, we employ the well-known Breuer-Laine-Piilo (BLP) measure [84] and generalize it to the discrete time evolution.

The idea of the BLP measure is to quantify the non-Markovianity through the trace distance change of the system state as follows:

$$\mathcal{N} = \max_{\rho_1, \rho_2} \sum_{\Delta \mathcal{D}(n) > 0} \Delta \mathcal{D}(n), \quad (24)$$

with  $\Delta \mathcal{D}(n) = \mathcal{D}[\rho_1(n+1), \rho_2(n+1)] - \mathcal{D}[\rho_1(n), \rho_2(n)]$  and  $\mathcal{D}(\rho_1, \rho_2) = \text{tr}(\sqrt{(\rho_1 - \rho_2)^\dagger(\rho_1 - \rho_2)})/2$  is the trace distance between the two density matrices  $\rho_1$  and  $\rho_2$ . The trace distance quantifies the degree of distinguishability between the two states with  $0 \leq \mathcal{D}(\rho_1, \rho_2) \leq 1$  and  $\mathcal{D}(\rho_1, \rho_2) = 1$  corresponds to the case where the two states are orthogonal. In the Markovian process, because the information of the system is one-way flows into the environment, all distinct initial states will eventually approach a unique steady state manifested by  $\Delta \mathcal{D}(n) < 0$  for all  $n$ . However, if  $\Delta \mathcal{D}(n) > 0$  exists for some  $n$ , namely, the distinguishability of the two initial states increases, it is a signal that the information have flowed back to the system at some point and thus the dynamics is non-Markovian. The non-Markovianity is obtained by the sum of all the increases of the trace distance during the time evolution.

In principle, the maximization in Eq. (24) should run over all the possible initial states. Here we performed  $K = 200$  simulations, with  $\rho_1$  being a random state and  $\rho_2 = \rho_1^\perp$  being the orthogonal state of  $\rho_1$ . The non-Markovianity  $\mathcal{N}$  is thus given by the optimal pair of  $\rho_1$  and  $\rho_2$  within all the performed simulations. The non-Markovianity  $\mathcal{N}$  as a function of the strength of the  $E_n-E_{n+1}$  collision  $\theta$  is shown in Fig. 6. Note that according to the equation  $\theta = 2g_E\tau$  in Sec. II, the

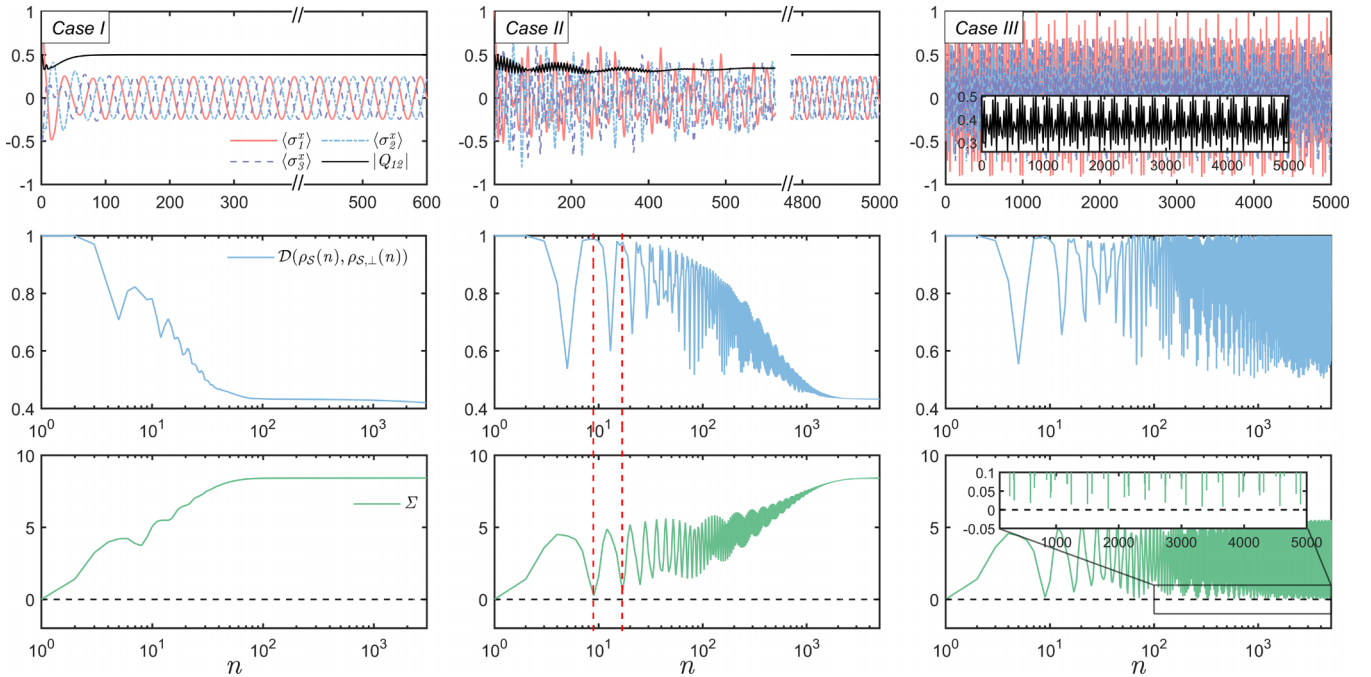


FIG. 7. The time evolution of the expectation values of  $\langle \sigma_m^x \rangle$  ( $m = 1, 2, 3$ ) and the modulus of the synchronization measure  $Q_{12}$  (top panels), the trace distance  $\mathcal{D}[\rho_S(n), \rho_{S,\perp}(n)]$  (middle panels), and entropy production  $\Sigma$  (bottom panels) for case I: weak non-Markovian case with  $\theta = \pi/3$ ; case II: strong non-Markovian case with  $\theta = \pi/2.1$ ; and case III: ultrastrong non-Markovian case with  $\theta = \pi/2$ . The initial state of the system is chosen as  $\rho_1$  to be the  $120^\circ$  state and  $\rho_2$  to be the orthogonal state of  $\rho_1$ , i.e.,  $\mathcal{D}(\rho_S^{\text{ini}}, \rho_{S,\perp}^{\text{ini}}) = 1$ . Other parameters are chosen as  $J_x = J_y = -1, J_z = 1, \beta = 10, g = 5$ , and  $\tau = 0.08$ .

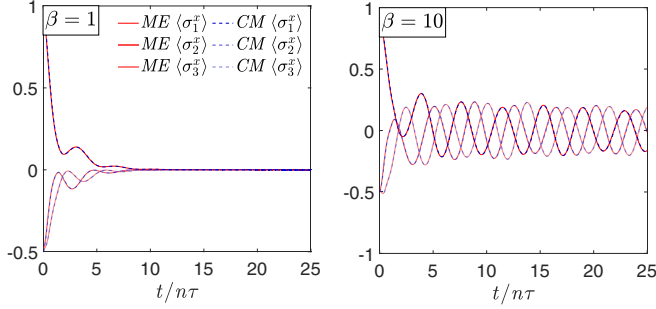


FIG. 8. The time evolution of  $\langle \sigma_m^x \rangle$  ( $m = 1, 2, 3$ ) of the system  $\mathcal{S}$  (the subsystems are distinguished by the transparency of the lines) in the description of master equation (A5) and the collision model for  $\beta = 1$  (left) and 10 (right). Other parameters are chosen as  $J_x = J_y = -1$ ,  $J_z = 1$ ,  $g = 10$ , and  $\tau = 0.01$ .

coupling strength between environmental spins is proportional to  $\theta$ . One can find that the non-Markovianity of the dynamics is not induced as soon as the  $E_n$ - $E_{n+1}$  collision is switched on. When the  $E_n$ - $E_{n+1}$  collision is weak, e.g.,  $\theta/\pi < 0.2$ , after  $n = 500$  collisions, the non-Markovianity  $\mathcal{N}$  is always zero. As we continue to increase the strength of the  $E_n$ - $E_{n+1}$  collision, the dynamics becomes non-Markovian and  $\mathcal{N}$  increases monotonically with  $\theta$  increasing.

For the non-Markovian region ( $\theta/\pi = 0.2$ ), we discuss the following three cases:

*Case I.* The weak non-Markovian case with  $\theta = \pi/3$ .

*Case II.* The strong non-Markovian case with  $\theta = \pi/2.1$ .

*Case III.* The ultrastrong non-Markovian case with  $\theta = \pi/2$ .

Meanwhile, the unitary-evolution operator within the environment blocks  $U_{E_n E_{n+1}}$  is the SWAP gate when  $\theta = \pi/2$ . The state of the system is initialized to the  $120^\circ$  state. As for initial states of the system in the calculation of the trace distance  $\mathcal{D}(\rho_1, \rho_2)$ , the state  $\rho_1$  is the  $120^\circ$  state and the other one is the orthogonal state of  $\rho_2 = \rho_1^\perp$ .

Since the correlation between environment blocks has been established in the non-Markovian case, we have to redefine the entropy production before proceeding to a specific discussion. What is noteworthy in the non-Markovian case is that in each collision cycle, two environment blocks are involved. To be more precise, the detailed expression of the interval entropy flux in each collision cycle has to contain the total energy of those two environment parts [85], that is,

$$\Phi^n = \beta \Delta Q_E^n = \beta \text{tr}[(H_n \otimes H_{n+1})(\rho_{E_n E_{n+1}}^{\text{post}} - \rho_{E_n E_{n+1}}^{\text{pre}})]. \quad (25)$$

For the sake of understanding, let us recall the entail collision evolution introduced before:

$$\begin{aligned} \rho_{SE_n E_{n+1}}^{\text{pre}} &\equiv \rho_{SE_n} \otimes \eta_n^{n+1}, \\ \rho_{SE_n E_{n+1}}^{\text{post}} &\equiv U_E U_I U_S \rho_{SE_n E_{n+1}}^{\text{pre}} U_S^\dagger U_I^\dagger U_E^\dagger. \end{aligned} \quad (26)$$

Here, once again, to avoid misunderstanding, we emphasize that  $H$  is the free Hamiltonian of the thermal environment particle.

In Fig. 7, we show the time evolution of  $\langle \sigma_m^x \rangle$  and the modulus of the synchronization measure  $Q_{12}$ . For the weak non-Markovian case, one can find that the dynamics of the

system do not suffer from non-Markovianity and oscillations can be rapidly built up in the evolution. As shown in the left-middle panel of Fig. 7, although the dynamic is non-Markovian, the information backflow ( $\Delta \mathcal{D} > 0$ ) only occurs in the early stage of the evolution and then the trace distance decreases monotonically. As for the entropy production, in case I, the entropy production is always a positive value, which is far from a zero value and rapidly reaches a constant. The phenomena are similar to the Markovian case, and a subspace of the system will rapidly decouple from the environment during evolution and the weak non-Markovianity does not have a significant effect on the system dynamic.

In case II, by contrast, both the expectation values of  $\langle \sigma_m^x \rangle$  and  $|Q_{12}|$  show irregular oscillations at the beginning of the evolution; see the second column of Fig. 7. In spite of the early-stage haphazard behavior, the system evolution gradually becomes regular and stabilizes around  $n = 2500$  (not shown in Fig. 7), and the system eventually reaches stable oscillations. The modulus of the quantum synchronization measure  $|Q_{12}|$  also reaches a constant value in the long-time evolution, which hints at the existence of good synchronization. The time dependence of the trace distance for case II shows a rapid oscillation until  $n > 1000$ , which is a typical evidence for the strong non-Markovian dynamics. In particular, at some moments (marked by red dashed lines), the trace distance instantaneously recovers the initial value.

The strong non-Markovianity significantly impacts the entropy production in the time evolution. One can see that the entropy production does not monotonically increase and may decrease drastically close to zero at some  $n$  in the discrete time evolution. This indicates that the entropy production at the  $n$ th step  $\Sigma^n$  becomes negative. This can be understood by, for example, focusing on the steps  $n = 9$  and  $17$  (the red dashed lines in Fig. 7) at which the trace distance (almost) recovers to unity; it is the strong information backflow that diminishes the vague of different states and decreases the entropy of the system and thus leads to the negative  $\Sigma^n$  at  $n = 9$  and  $17$ . But when we look at  $\Sigma(n)$  through the entire time evolution, the boundary of violation of the second law of thermodynamics is untouchable [85].

In case III, the collision between neighboring environmental spins is set to be the SWAP operation. As shown in the right column of Fig. 7, one can find that the dynamics of the system always exhibit irregular oscillations, even in the long-time limit ( $n \sim 5000$ ). In addition, the measure  $|Q_{12}|$  fails to reach an asymptotic steady-state value, implying the absence of synchronization in such ultrastrong non-Markovian dynamics. The time dependence of both the trace distance as well as the entropy production oscillate irregularly. Again, the nonmonotonic behavior of the entropy production is observed in the ultrastrong non-Markovian case. The negative entropy production  $\Sigma^n$  during the time evolution is due to the creation of the correlations in the system and environmental qubits [82,85].

We would finish by emphasizing again that in the CM scenario, since the thermal environment is represented by a series of qubits, the thermodynamic quantities should be the cumulation of the same quantities at each step to ensure all the changes in the involved environmental qubits are taken

into account. In this sense, the second law of thermodynamics still holds in our model from a macroscopic point of view.

## V. SUMMARY

In summary, we have investigated the dissipative dynamics of a tripartite spin system in the framework of the CM. With the introduction of successive collisions between the system and environment spins, collective dissipation has been simulated. We have found that when the environment temperature is low, the dynamics of the system exhibit a well-defined oscillation and the mutual synchronization can be established among the subsystems. We proceeded the discussion by classifying the present CM into the Markovian and the non-Markovian cases, according to whether or not the collision between neighboring environmental spins is allowed.

In the Markovian case, we have discussed the effects of the coupling strength and environment temperature on the dynamics of the systems, as well as the property of synchronization among subsystems. We find that the dynamics of the system may show periodical oscillations when the environmental temperature is low and the anisotropy of the interactions between the subsystems tends to destroy the stable oscillation. In addition, we have extracted the frequency of the oscillation by means of FFT.

To understand the establishment of the stable oscillations in the Markovian dynamics, we have connected the descriptions of the CM and master equation by virtue of taking the continuous-time limit on the interval collisions. We then analyzed the Liouvillian spectrum of the master equation and found that there indeed exist purely imaginary eigenvalues when the environment temperature is low. In particular, the inverse of the modulus of the pure imaginary eigenvalues is consistent with the oscillation frequency accessed by the FFT. We further investigated the structure of the density matrix of the system and found that the system's oscillatory behavior is actually a process of leapfrogging between degenerate Hamiltonian eigenstates and other energy eigenstates

within a subspace consisting of eigenoperators. Finally, we investigated the temporal behaviors of entropy production and quantum correlations, which shows the oscillation of the system is induced not only by the coupling to the environment, but also as a result of self-adjusting the correlations among the subsystems. We also discussed the effects of the imperfection of the collective interactions on the long-time oscillations.

For the non-Markovian case, we utilized the BLP measure of non-Markovianity in the stroboscopic time evolution in the CM. We found, in the strong (and ultrastrong) non-Markovian dynamics, that the entropy production is always positive and may exhibit nonmonotonic behavior in the time evolution, implying that the entropy production in some collision steps becomes negative. This can be understood by the fact that the backflow of information in strong non-Markovianity dynamics compensates the energy in erasing the information. Finally, the dynamic of the system exhibits chaoslike behavior, even after a sufficiently long time in the ultrastrong non-Markovian case. In future work, it will be interesting to check the chaotic behavior of the system and investigate the influence of the system-environment correlations on the system dynamics behavior.

## ACKNOWLEDGMENT

This work is supported by National Natural Science Foundation of China under Grant No. 11975064.

## APPENDIX

In this Appendix, we take the collision sequence given in Sec. III E as an example to show the specific form of the master equation for the sequential collision case. Here we recall the unitary-evolution operator  $U_{I,123}^{\text{seq}} = U_{S_3 E_n} U_{S_2 E_n} U_{S_1 E_n}$ , with  $U_{S_m E_n} = \exp[-ig\tau(\sigma_{S_m}^+ \sigma_{E_n}^- + \text{H.c.})]$  ( $m = 1, 2, 3$ ), and the environment particles are still located in the thermal state without off-diagonal matrix elements.

The dynamical map for the system also can be given by

$$\rho_S^n \mapsto \rho_S^{n+1} = \text{tr}_{E_{n+1}} [U_{I,123}^{\text{seq}} U_S(\rho_S^n \otimes \eta_{\text{th}}^{n+1}) U_S^\dagger U_{I,123}^{\text{seq},\dagger}] = \Lambda[\rho_S^n]. \quad (\text{A1})$$

Based on the requirements of the continuous-time limit, which hints at  $\tau \rightarrow 0$ , we still expand the unitary operators as follows:

$$U_{S_m E_n} = \mathbb{I} - i\tau V_m - \tau^2 V_m^2/2 + o(\tau^n) \approx \mathbb{I} - ig\tau(\sigma_{S_m}^+ \sigma_{E_n}^- + \text{H.c.}) - g^2 \tau^2 (\sigma_{S_m}^+ \sigma_{E_n}^- + \text{H.c.})^2/2, \quad (\text{A2})$$

and

$$U_S = \mathbb{I} - i\tau H_S + o(\tau^n). \quad (\text{A3})$$

Then we can directly obtain the mapping of the collision,

$$\begin{aligned} \rho_S^{n+1} = \Lambda[\rho_S^n] = \text{tr}_{E_n} [U_{S_3 E_n} U_{S_2 E_n} U_{S_1 E_n} U_S(\rho_S^n \otimes \eta_{\text{th}}^{n+1}) U_S^\dagger U_{S_1 E_n} U_{S_2 E_n} U_{S_3 E_n}] = \text{tr}_{E_n} \left[ \left\{ \mathbb{I} - i\tau(V_1 + V_2 + V_3 + H_S) \right. \right. \\ \left. \left. - \frac{\tau^2}{2}(V_1^2 + V_2^2 + V_3^2) - \tau^2(V_3 V_2 + V_2 V_1 + V_3 V_1) - \tau^2(V_3 + V_2 + V_1)H_S \right\} \cdot \{\rho_S^n \otimes \eta_{\text{th}}^{n+1}\} \right. \\ \left. \times \left\{ \mathbb{I} + i\tau(V_1 + V_2 + V_3 + H_S) - \frac{\tau^2}{2}(V_1^2 + V_2^2 + V_3^2) - \tau^2(V_2 V_3 + V_1 V_2 + V_1 V_3) - \tau^2 H_S(V_3 + V_2 + V_1) \right\} \right]. \quad (\text{A4}) \end{aligned}$$

Recall the timescale  $\tau \rightarrow 0$  and  $g^2\tau = \text{const.}$  We have

$$\begin{aligned}
\rho_S^{n+1} &= \text{tr}_{E_n} \left[ \rho_S^n \otimes \eta_{\text{th}}^{n+1} - i\tau H_S(\rho_S^n \otimes \eta_{\text{th}}^{n+1}) - \frac{\tau^2}{2}(V_1^2 + V_2^2 + V_3^2)(\rho_S^n \otimes \eta_{\text{th}}^{n+1}) - \tau^2(V_3V_2 + V_2V_1 + V_3V_1)(\rho_S^n \otimes \eta_{\text{th}}^{n+1}) \right. \\
&\quad \left. + i\tau(\rho_S^n \otimes \eta_{\text{th}}^{n+1})H_S + \tau^2(V_3 + V_2 + V_1)(\rho_S^n \otimes \eta_{\text{th}}^{n+1})(V_1 + V_2 + V_3) - \frac{\tau^2}{2}(\rho_S^n \otimes \eta_{\text{th}}^{n+1})(V_1^2 + V_2^2 + V_3^2) \right] \\
&= \rho_S^n - i\tau[H_S, \rho_S^n] + \frac{g^2\tau^2}{2} \sum_m \langle \sigma_{E_n}^+ \sigma_{E_n}^+ \rangle_{\eta_{\text{th}}^{n+1}} (2\sigma_m^- \rho_S^n \sigma_m^- - \{\sigma_m^- \sigma_m^-, \rho_S^n\}) + \frac{g^2\tau^2}{2} \sum_m \langle \sigma_{E_n}^- \sigma_{E_n}^- \rangle_{\eta_{\text{th}}^{n+1}} (2\sigma_m^+ \rho_S^n \sigma_m^+ - \{\sigma_m^+ \sigma_m^+, \rho_S^n\}) \\
&\quad + \frac{g^2\tau^2}{2} \sum_m \langle \sigma_{E_n}^- \sigma_{E_n}^+ \rangle_{\eta_{\text{th}}^{n+1}} (2\sigma_m^- \rho_S^n \sigma_m^+ - \{\sigma_m^+ \sigma_m^-, \rho_S^n\}) + \frac{g^2\tau^2}{2} \sum_m \langle \sigma_{E_n}^+ \sigma_{E_n}^- \rangle_{\eta_{\text{th}}^{n+1}} (2\sigma_m^+ \rho_S^n \sigma_m^- - \{\sigma_m^- \sigma_m^+, \rho_S^n\}) \\
&\quad + \frac{g^2\tau^2}{2} \sum_{m \neq k} \langle \sigma_{E_n}^+ \sigma_{E_n}^+ \rangle_{\eta_{\text{th}}^{n+1}} (2\sigma_m^- \rho_S^n \sigma_k^- - \sigma_m^- \sigma_k^- \rho_S^n - \rho_S^n \sigma_k^- \sigma_m^-) + \frac{g^2\tau^2}{2} \sum_{m \neq k} \langle \sigma_{E_n}^- \sigma_{E_n}^- \rangle_{\eta_{\text{th}}^{n+1}} (2\sigma_m^+ \rho_S^n \sigma_k^+ - \sigma_m^+ \sigma_k^+ \rho_S^n - \rho_S^n \sigma_k^+ \sigma_m^+) \\
&\quad + \frac{g^2\tau^2}{2} \sum_{m > k} \langle \sigma_{E_n}^+ \sigma_{E_n}^- \rangle_{\eta_{\text{th}}^{n+1}} (2\sigma_m^+ \rho_S^n \sigma_k^- - \sigma_m^- \sigma_k^+ \rho_S^n - \rho_S^n \sigma_k^- \sigma_m^+) + \frac{g^2\tau^2}{2} \sum_{m > k} \langle \sigma_{E_n}^- \sigma_{E_n}^+ \rangle_{\eta_{\text{th}}^{n+1}} (2\sigma_m^- \rho_S^n \sigma_k^+ - \sigma_m^+ \sigma_k^- \rho_S^n - \rho_S^n \sigma_k^+ \sigma_m^-) \\
&\quad + \frac{g^2\tau^2}{2} \sum_{m < k} \langle \sigma_{E_n}^- \sigma_{E_n}^+ \rangle_{\eta_{\text{th}}^{n+1}} (2\sigma_m^+ \rho_S^n \sigma_k^- - \sigma_m^- \sigma_k^+ \rho_S^n - \rho_S^n \sigma_k^- \sigma_m^+) + \frac{g^2\tau^2}{2} \sum_{m < k} \langle \sigma_{E_n}^+ \sigma_{E_n}^- \rangle_{\eta_{\text{th}}^{n+1}} (2\sigma_m^- \rho_S^n \sigma_k^+ - \sigma_m^+ \sigma_k^- \rho_S^n - \rho_S^n \sigma_k^+ \sigma_m^-).
\end{aligned} \tag{A5}$$

In the above equation, the terms with  $\tau^2$  and  $g\tau^2$  are all neglected, and the summations run over  $m, k = 1, 2, 3$ . We have to especially emphasize that the relation between  $m$  and  $k$  in the summations is related to and satisfies the current collision sequence. Then, we again emphasize the specific form of the state of the environment particle; the state without the off-diagonal elements will lead to  $\langle \sigma_{E_n}^+ \sigma_{E_n}^+ \rangle_{\eta_{\text{th}}^{n+1}} = \langle \sigma_{E_n}^- \sigma_{E_n}^- \rangle_{\eta_{\text{th}}^{n+1}} = 0$ , and the results of  $\langle \sigma_{E_n}^- \sigma_{E_n}^+ \rangle_{\eta_{\text{th}}^{n+1}} = (1 - \xi)/2$  and  $\langle \sigma_{E_n}^+ \sigma_{E_n}^- \rangle_{\eta_{\text{th}}^{n+1}} = (1 + \xi)/2$  with  $\xi = \tanh(-\beta\omega)$ . The parameters  $\beta$  and  $\omega$  are environmental conditions which we have mentioned in Sec. III E. We also present the comparison of the above master equation and the CM in Fig. 8. Following the identical method in the previous section, we still consider

the environment state in low temperature, e.g.,  $\xi \approx -1$ , and we can finally obtain the master equation,

$$\begin{aligned}
\frac{d}{dt} \rho_S(t) &= -i[H_S, \rho_S(t)] + \frac{\gamma}{2} [2A^- \rho_S(t) A^+ - \{\rho_S(t), A^+ A^-\}] \\
&\quad + \frac{\gamma}{2} [\sigma_2^+ \sigma_3^- + \sigma_1^+ \sigma_3^- + \sigma_1^+ \sigma_2^-, \rho_S(t)] \\
&\quad + \frac{\gamma}{2} [\rho_S(t), \sigma_3^+ \sigma_2^- + \sigma_3^+ \sigma_1^- + \sigma_2^+ \sigma_1^-],
\end{aligned} \tag{A6}$$

where  $A^\pm = \sum_m \sigma_m^\pm$  are the collective lowering and raising operators. The corresponding Liouvillian spectrum is shown in the zoom-in of Fig. 5, which hints that the system is unable to govern the stable oscillations.

- 
- [1] H.-P. Breuer and F. Petruccione, *The Theory of Open Quantum Systems* (Oxford University Press, Oxford, 2002).
- [2] Á. Rivas and S. F. Huelga, *Open Quantum Systems*, Vol. 10 (Springer, Berlin, 2012).
- [3] H.-P. Breuer, E.-M. Laine, J. Piilo, and B. Vacchini, Colloquium: Non-Markovian dynamics in open quantum systems, *Rev. Mod. Phys.* **88**, 021002 (2016).
- [4] L. Banchi, P. Giorda, and P. Zanardi, Quantum information-geometry of dissipative quantum phase transitions, *Phys. Rev. E* **89**, 022102 (2014).
- [5] D. Maile, S. Andergassen, W. Belzig, and G. Rastelli, Quantum phase transition with dissipative frustration, *Phys. Rev. B* **97**, 155427 (2018).
- [6] M.-J. Hwang, P. Rabl, and M. B. Plenio, Dissipative phase transition in the open quantum Rabi model, *Phys. Rev. A* **97**, 013825 (2018).
- [7] M. Prasad, H. K. Yadalam, C. Aron, and M. Kulkarni, Dissipative quantum dynamics, phase transitions, and non-Hermitian random matrices, *Phys. Rev. A* **105**, L050201 (2022).
- [8] Y.-L. Zhang, Y. Huang, and X. Chen, Information scrambling in chaotic systems with dissipation, *Phys. Rev. B* **99**, 014303 (2019).
- [9] G. Styliaris, N. Anand, and P. Zanardi, Information Scrambling over Bipartitions: Equilibration, Entropy Production, and Typicality, *Phys. Rev. Lett.* **126**, 030601 (2021).
- [10] P. Zanardi and N. Anand, Information scrambling and chaos in open quantum systems, *Phys. Rev. A* **103**, 062214 (2021).
- [11] A. C. Potter, R. Vasseur, and S. A. Parameswaran, Universal Properties of Many-Body Delocalization Transitions, *Phys. Rev. X* **5**, 031033 (2015).
- [12] K. Hyatt, J. R. Garrison, A. C. Potter, and B. Bauer, Many-body localization in the presence of a small bath, *Phys. Rev. B* **95**, 035132 (2017).



- [13] A. R.-Abadal, J.-y. Choi, J. Zeiher, S. Hollerith, J. Rui, I. Bloch, and C. Gross, Many-Body Delocalization in the Presence of a Quantum Bath, *Phys. Rev. X* **9**, 041014 (2019).
- [14] X. Xu and D. Poletti, Localization-delocalization effects of a delocalizing dissipation on disordered XXZ spin chains, *Chaos* **31**, 033133 (2021).
- [15] F. Wilczek, Quantum Time Crystals, *Phys. Rev. Lett.* **109**, 160401 (2012).
- [16] V. K. Kozin and O. Kyriienko, Quantum Time Crystals from Hamiltonians with Long-Range Interactions, *Phys. Rev. Lett.* **123**, 210602 (2019).
- [17] G. Engelhardt, A classical view of quantum time crystals, *Physics* **14**, 132 (2021).
- [18] Q. Zhuang and B. Wu, Equilibration of quantum chaotic systems, *Phys. Rev. E* **88**, 062147 (2013).
- [19] W. Bruzda, M. Smaczyński, V. Cappellini, H.-J. Sommers, and K. Życzkowski, Universality of spectra for interacting quantum chaotic systems, *Phys. Rev. E* **81**, 066209 (2010).
- [20] A. W. Laskar, P. Adhikary, S. Mondal, P. Katiyar, S. Vinjanampathy, and S. Ghosh, Observation of Quantum Phase Synchronization in Spin-1 Atoms, *Phys. Rev. Lett.* **125**, 013601 (2020).
- [21] N. Jaseem, M. Hajdušek, P. Solanki, L.-C. Kwek, R. Fazio, and S. Vinjanampathy, Generalized measure of quantum synchronization, *Phys. Rev. Res.* **2**, 043287 (2020).
- [22] P. Solanki, N. Jaseem, M. Hajdušek, and S. Vinjanampathy, Role of coherence and degeneracies in quantum synchronization, *Phys. Rev. A* **105**, L020401 (2022).
- [23] M. Hajdušek, P. Solanki, R. Fazio, and S. Vinjanampathy, Seeding Crystallization in Time, *Phys. Rev. Lett.* **128**, 080603 (2022).
- [24] V. R. Krithika, P. Solanki, S. Vinjanampathy, and T. S. Mahesh, Observation of quantum phase synchronization in a nuclear-spin system, *Phys. Rev. A* **105**, 062206 (2022).
- [25] O. V. Zhirov and D. L. Shepelyansky, Synchronization and Bistability of a Qubit Coupled to a Driven Dissipative Oscillator, *Phys. Rev. Lett.* **100**, 014101 (2008).
- [26] O. V. Zhirov and D. L. Shepelyansky, Quantum synchronization and entanglement of two qubits coupled to a driven dissipative resonator, *Phys. Rev. B* **80**, 014519 (2009).
- [27] F. Galve, L. A. Pachón, and D. Zueco, Bringing Entanglement to the High Temperature Limit, *Phys. Rev. Lett.* **105**, 180501 (2010).
- [28] S. Walter, A. Nunnenkamp, and C. Bruder, Quantum Synchronization of a Driven Self-Sustained Oscillator, *Phys. Rev. Lett.* **112**, 094102 (2014).
- [29] V. Ameri, M. Eghbali-Arani, A. Mari, A. Farace, F. Kheirandish, V. Giovannetti, and R. Fazio, Mutual information as an order parameter for quantum synchronization, *Phys. Rev. A* **91**, 012301 (2015).
- [30] G. Karpat, İ. Yalçınkaya, and B. Çakmak, Quantum synchronization in a collision model, *Phys. Rev. A* **100**, 012133 (2019).
- [31] A. Cabot, F. Galve, and R. Zambrini, Dynamical and quantum effects of collective dissipation in optomechanical systems, *New J. Phys.* **19**, 113007 (2017).
- [32] M. Ludwig and F. Marquardt, Quantum Many-Body Dynamics in Optomechanical Arrays, *Phys. Rev. Lett.* **111**, 073603 (2013).
- [33] C. C. Rodrigues, C. M. Kersul, A. G. Primo, M. Lipson, T. P. M. Alegre, and G. S. Wiederhecke, Optomechanical synchronization across multi-octave frequency spans, *Nat. Commun.* **12**, 5625 (2021).
- [34] C. Davis-Tilley, C. K. Teoh, and A. D. Armour, Dynamics of many-body quantum synchronisation, *New J. Phys.* **20**, 113002 (2018).
- [35] M. H. Xu, D. A. Tieri, E. C. Fine, J. K. Thompson, and M. J. Holland, Synchronization of Two Ensembles of Atoms, *Phys. Rev. Lett.* **113**, 154101 (2014).
- [36] V. M. Vinokur, T. I. Baturina, M. V. Fistul, A. Yu. Mironov, M. R. Baklanov, and C. Strunk, Superinsulator and quantum synchronization, *Nature (London)* **452**, 613 (2008).
- [37] F. Quijandría, D. Porras, and J. J. García-Ripoll, Circuit QED Bright Source for Chiral Entangled Light Based on Dissipation, *Phys. Rev. Lett.* **111**, 073602 (2013).
- [38] M. V. Fistul, Quantum synchronization in disordered superconducting metamaterials, *Sci. Rep.* **7**, 43657 (2017).
- [39] J. Rau, Relaxation Phenomena in Spin and Harmonic Oscillator Systems, *Phys. Rev.* **129**, 1880 (1963).
- [40] M. Ziman, P. Štelmachovič, V. Bužek, M. Hillery, V. Scarani, and N. Gisin, Diluting quantum information: An analysis of information transfer in system-reservoir interactions, *Phys. Rev. A* **65**, 042105 (2002).
- [41] V. Scarani, M. Ziman, P. Štelmachovič, N. Gisin, and V. Bužek, Thermalizing Quantum Machines: Dissipation and Entanglement, *Phys. Rev. Lett.* **88**, 097905 (2002).
- [42] M. Ziman and V. Bužek, All (qubit) decoherences: Complete characterization and physical implementation, *Phys. Rev. A* **72**, 022110 (2005).
- [43] F. Ciccarello, G. M. Palm, and V. Giovannetti, Collision-model-based approach to non-Markovian quantum dynamics, *Phys. Rev. A* **87**, 040103(R) (2013).
- [44] M. Cattaneo, G. De Chiara, S. Maniscalco, R. Zambrini, and G. L. Giorgi, Collision Models Can Efficiently Simulate Any Multipartite Markovian Quantum Dynamics, *Phys. Rev. Lett.* **126**, 130403 (2021).
- [45] M. Cattaneo, M. A. C. Rossi, G. García-Pérez, R. Zambrini, and S. Maniscalco, Quantum simulation of dissipative collective effects on noisy quantum computers, *PRX Quantum* **4**, 010324 (2023).
- [46] F. Ciccarello and V. Giovannetti, A quantum non-Markovian collision model: Incoherent SWAP case, *Phys. Scr.* **T153**, 014010 (2013).
- [47] R. McCloskey and M. Paternostro, Non-Markovianity and system-environment correlations in a microscopic collision model, *Phys. Rev. A* **89**, 052120 (2014).
- [48] J. Jin, V. Giovannetti, R. Fazio, F. Sciarrino, P. Mataloni, A. Crespi, and R. Osellame, All-optical non-Markovian stroboscopic quantum simulator, *Phys. Rev. A* **91**, 012122 (2015).
- [49] S. Lorenzo, F. Ciccarello, and G. M. Palma, Composite quantum collision models, *Phys. Rev. A* **96**, 032107 (2017).
- [50] J. Jin and C.-S. Yu, Non-Markovianity in the collision model with environmental block, *New J. Phys.* **20**, 053026 (2018).
- [51] R. R. Camasca and G. T. Landi, Memory kernel and divisibility of Gaussian collisional models, *Phys. Rev. A* **103**, 022202 (2021).

- [52] S. N. Filippov and I. A. Luchnikov, Collisional open quantum dynamics with a generally correlated environment: Exact solvability in tensor networks, *Phys. Rev. A* **105**, 062410 (2022).
- [53] F. Ciccarello, S. Lorenzo, V. Giovannetti, and G. M. Palma, Quantum collision models: Open system dynamics from repeated interactions, *Phys. Rep.* **954**, 1 (2022).
- [54] M. Cattaneo, G. L. Giorgi, R. Zambrini and S. Maniscalco, A brief journey through collision models for multipartite open quantum dynamics, *Open Syst. Inf. Dyn.* **29**, 2250015 (2022).
- [55] Y. Li and X. Li and J. Jin, Information scrambling in a collision model, *Phys. Rev. A* **101**, 042324 (2020).
- [56] Y. Li and X. Li and J. Jin, Dissipation-induced information scrambling in a collision model, *Entropy* **24**, 345 (2022).
- [57] K. Beyer, K. Luoma, and W. T. Strunz, Collision-model approach to steering of an open driven qubit, *Phys. Rev. A* **97**, 032113 (2018).
- [58] D. Grimmer, A. Kempf, R. B. Mann, and E. M.-Martínez, Zeno friction and antifricition from quantum collision models, *Phys. Rev. A* **100**, 042702 (2019).
- [59] B. Çakmak, S. Campbell, B. Vacchini, Ö. E. Müstecaplıoğlu, and M. Paternostro, Robust multipartite entanglement generation via a collision model, *Phys. Rev. A* **99**, 012319 (2019).
- [60] G. Karpat, İ. Yalçınkaya, B. Çakmak, G. L. Giorgi, and R. Zambrini, Synchronization and non-Markovianity in open quantum systems, *Phys. Rev. A* **103**, 062217 (2021).
- [61] Á. Cuevas, A. Gerdali, C. Liorni, L. D. Bonavena, A. D. Pasquale, F. Sciarrino, V. Giovannetti, and P. Mataloni, All-optical implementation of collision-based evolutions of open quantum systems, *Sci. Rep.* **9**, 3205 (2019).
- [62] G. Karpat, İ. Yalçınkaya, and B. Çakmak, Quantum synchronization of few-body systems under collective dissipation, *Phys. Rev. A* **101**, 042121 (2020).
- [63] A. V. Andreev, V. I. Emel'yanov, and Y. A. Il'inskiĭ, Collective spontaneous emission (Dicke superradiance), *Sov. Phys. Usp.* **23**, 493 (1980).
- [64] M. H. Levitt, *Spin Dynamics: Basics of Nuclear Magnetic Resonance*, 2nd ed. (Wiley, Chichester, 2012), pp. 369–408.
- [65] S. J. Masson and A. Asenjo-Garcia, Universality of Dicke superradiance in arrays of quantum emitters, *Nat. Commun.* **13**, 2285 (2022).
- [66] S. Schneider and G. J. Milburn, Entanglement in the steady state of a collective-angular-momentum (Dicke) model, *Phys. Rev. A* **65**, 042107 (2002).
- [67] T. E. Lee, C.-K. Chan, and S. F. Yelin, Dissipative phase transitions: Independent versus collective decay and spin squeezing, *Phys. Rev. A* **90**, 052109 (2014).
- [68] N. Es'haqi-Sani, G. Manzano, R. Zambrini, and R. Fazio, Synchronization along quantum trajectories, *Phys. Rev. Res.* **2**, 023101 (2020).
- [69] F. Galve, G. Luca Giorgi, and R. Zambrini, Quantum correlations and synchronization measures, in *Lectures on General Quantum Correlations and their Applications*, edited by F. Fernandes Fanchini, D. de Oliveira Soares Pinto, and G. Adesso (Springer International, Cham, Switzerland, 2017), pp. 393–420.
- [70] N. Jaseem, M. Hajdušek, V. Vedral, R. Fazio, L.-C. Kwek, and S. Vinjanampathy, Quantum synchronization in nanoscale heat engines, *Phys. Rev. E* **101**, 020201(R) (2020).
- [71] T. Baumgratz, M. Cramer, and M. B. Plenio, Quantifying Coherence, *Phys. Rev. Lett.* **113**, 140401 (2014).
- [72] E. M. Kessler, G. Giedke, A. Imamoglu, S. F. Yelin, M. D. Lukin, and J. I. Cirac, Dissipative phase transition in a central spin system, *Phys. Rev. A* **86**, 012116 (2012).
- [73] F. Minganti, A. Biella, N. Bartolo, and C. Ciuti, Spectral theory of Liouvillians for dissipative phase transitions, *Phys. Rev. A* **98**, 042118 (2018).
- [74] V. V. Albert and L. Jiang, Symmetries and conserved quantities in Lindblad master equations, *Phys. Rev. A* **89**, 022118 (2014).
- [75] B. Buča, J. Tindall, and D. Jaksch, Non-stationary coherent quantum many-body dynamics through dissipation, *Nat. Commun.* **10**, 1730 (2019).
- [76] G. Guarnieri, M. T. Mitchison, A. Purkayastha, D. Jaksch, B. Buča, and J. Goold, Time periodicity from randomness in quantum systems, *Phys. Rev. A* **106**, 022209 (2022).
- [77] B. Buča, C. Booker and D. Jaksch, Algebraic theory of quantum synchronization and limit cycles under dissipation, *SciPost Phys.* **12**, 097 (2022).
- [78] G. T. Landi and M. Paternostro, Irreversible entropy production: From classical to quantum, *Rev. Mod. Phys.* **93**, 035008 (2021).
- [79] P. Strasberg and A. Winter, First and second law of quantum thermodynamics: A consistent derivation based on a microscopic definition of entropy, *PRX Quantum* **2**, 030202 (2021).
- [80] A. Purkayastha, G. Guarnieri, S. Campbell, J. Prior, and J. Goold, Periodically refreshed quantum thermal machines, *Quantum* **6**, 801 (2022).
- [81] S. Lorenzo, R. McCloskey, F. Ciccarello, M. Paternostro, and G. M. Palma, Landauer's Principle in Multipartite Open Quantum System Dynamics, *Phys. Rev. Lett.* **115**, 120403 (2015).
- [82] Z.-X. Man, Y.-J. Xia, and R. L. Franco, Validity of the Landauer principle and quantum memory effects via collisional models, *Phys. Rev. A* **99**, 042106 (2019).
- [83] M. Esposito, K. Lindenberg, and C. V. D. Broeck, Entropy production as correlation between system and reservoir, *New J. Phys.* **12**, 013013 (2010).
- [84] H.-P. Breuer, E.-M. Laine, and J. Piilo, Measure for the Degree of Non-Markovian Behavior of Quantum Processes in Open Systems, *Phys. Rev. Lett.* **103**, 210401 (2009).
- [85] M. Pezzutto, M. Paternostro and Y. Omar, Implications of non-Markovian quantum dynamics for the Landauer bound, *New J. Phys.* **18**, 123018 (2016).